

Simulating the transport and dispersal of volcanic ash clouds with initial conditions created by a 3D plume model

Zhixuan Cao^{1,2} Marcus Bursik³ Qingyuan Yang^{4,5} Abani Patra^{*,1,6}

¹ *Mechanical and Aerospace Engineering Department, SUNY Buffalo, Buffalo, NY, USA*

² *Fluids Business Unit, ANSYS Inc, Lebanon, NH, USA*

³ *Center for Geohazards Studies, SUNY Buffalo, Buffalo, NY, USA*

⁴ *Earth Observatory of Singapore, Singapore, Singapore*

⁵ *The Asian School of the Environment, Nanyang Technological University, Singapore, Singapore*

⁶ *Data Intensive Studies Center, Tufts University, Medford, MA, USA*

Correspondence*:

Abani Patra

abani.patra@tufts.edu

2 ABSTRACT

VATD (volcanic ash transport and dispersion) models simulate atmospheric transport of ash starting from a source originating at the volcano represented by concentration of ash with height. Most VATD models use a source of some prescribed shape calibrated against an empirical expression for the height-mass eruption rate (MER) relation. The actual vertical ash distribution in volcanic plumes usually varies from case to case and have complex dependencies on eruption source parameters and atmospheric conditions. We present here for the first time the use of a 3D (three-dimensional) plume model to represent the ash cloud source without any assumption regarding plume geometry. By eliminating assumed behavior associated with a semi-empirical plume geometry, the predictive skill of VATD simulations is greatly improved. To date, no VATD simulation adopts initial conditions created from first principles based on a 3D plume simulation. We use our recently developed volcanic plume model based on a 3D smoothed-particle hydrodynamic Lagrangian method, and couple the output to a standard Lagrangian VATD model. We apply the coupled model to the Pinatubo eruption in 1991 to illustrate the effectiveness of the approach. Our investigation reveals that initial particle distribution in the vertical direction has more impact on transport of ash clouds than does the horizontal distribution. Comparison with satellite data indicates that ash particles are concentrated through the depth of the volcanic umbrella cloud, and much lower than the observed maximum plume height.

20 Keywords: VATD, volcano, 3D plume model, initial conditions, numerical simulation, SPH, Pinatubo, ash transport, ash dispersal

1 INTRODUCTION

Volcanic ash, the fine-grained fraction of tephra, can be widely dispersed to synoptic and global scales, and can lead to a degradation of air quality and pose threats to aviation (Tupper et al., 2007). Identification, tracking and modeling the future movement of volcanic ash help route and schedule flights to avoid ash

24 clouds. Numerical estimation of ash distribution using known and forecast wind fields is necessary if we
25 are to accurately predict ash cloud propagation and spread. Numerous VATD (volcanic ash transport and
26 dispersion) models have been developed by both civil and military aviation, and meteorological agencies
27 to provide forecasts of ash cloud motion (Witham et al., 2007), such as Puff (Tanaka, 1991; Searcy et al.,
28 1998), VAFTAD (Heffter and Stunder, 1993), Tephra (Bonadonna et al., 2005), HYSPLIT(Stein et al.,
29 2015; Rolph et al., 2017) and Ash3d (Schwaiger et al., 2012). New techniques have been integrated into
30 VATDs to satisfy increasing demands for different types of output, model accuracy and forecast reliability.
31 This contribution explores a method for creating initial conditions for VATD simulations, which promises
32 to improve prediction capability.

33 Fero et al. (2009) and Stohl et al. (2011) showed that initial source conditions have significant effects
34 on simulation of volcanic ash transport. Besides location of the eruption vent and timings of the release,
35 traditional VATD simulation requires key global descriptors of the volcanic plume, especially plume height,
36 grain size, eruption duration and mass loading, or alternatively, a mass eruption rate (MER). No matter
37 how these global descriptors are obtained, they are used to furnish the initial conditions for VATDs in the
38 form of a line-source term of a spatio-temporal distribution of particle mass. It is a common practice to
39 pick values for these global descriptors using an empirical expression for the height-MER relation. The
40 empirical expression is written as a function of several parameters, including the key global descriptors.
41 The values for the descriptors can also be found by parameter calibration (e.g. Fero et al., 2008, 2009;
42 Stohl et al., 2011; Zidikheri et al., 2017). One-dimensional (1D) plume models serve as an alternative
43 option to provide values. For example, Bursik et al. (2012) used the 1D model puffin (Bursik, 2001) to
44 generate estimates of mass eruption rate and grain size. In some cases, an extra step is adopted to spread
45 ash particles from the line source horizontally, resulting in an initial ash cloud in 3D space. The horizontal
46 spreading depends on an empirical expression. For example, the VATD model Puff spreads particles from
47 the line source uniformly in the horizontal direction within a given radius using an empirical expression
48 generated from the output of puffin. Considering the complexities of volcanic eruptions, the actual ash
49 distribution in the initial ash cloud should vary from case to case and with time, making it difficult to find
50 one general expression that is suitable for all cases. It is useful therefore to investigate alternative ways for
51 creating initial ash clouds without assumptions regarding plume geometry, or numerical inversion. This
52 provides the major motivation of this paper.

53 VATD models can be categorized into Lagrangian particle tracking and Eulerian advection-diffusion types.
54 Among several available particle tracking models, such as, Hypact (Walko et al., 1995), Puff (Searcy et al.,
55 1998), CANERM (D'amours, 1998), and HYSPLIT (Draxler and Hess, 1998) and advection-diffusion
56 models, such as, Tephra (Bonadonna and Houghton, 2005), Fall3D (Folch et al., 2009), and Ash3D
57 (Schwaiger et al., 2012), we adopt a particle tracking model, Puff, as the primary VATD model. Puff
58 can accept a 3D point cloud description of the starting ash cloud as an initial condition, which makes
59 it technically easier to couple with 3D plume models. Puff initializes a discrete number of tracers that
60 represent a sample of the eruption cloud, and calculates transport, turbulent dispersion, and fallout for each
61 representative tracer. A cylinder emanating vertically from the volcano summit to a specified maximum
62 height is the standard approach to provide a simple model of the geometry of a typical ash column. Puff
63 minimally requires horizontal wind field data. The “restart” feature of Puff makes it technically feasible to
64 accommodate the hand-off between a plume simulation and the Puff simulation in terms of time and length
65 scales.

66 We also implement one of the most widely used models for atmospheric trajectory and dispersion
67 calculations, the Hybrid Single-Particle Lagrangian Integrated Trajectory model (HYSPLIT) (Stein et al.,

68 2015; Rolph et al., 2017), developed by NOAA's Air Resources Laboratory. HYSPLIT is able to simulate
69 phenomena from simple back trajectories, to very sophisticated computations of transport, mixing, chemical
70 transformation, and deposition of pollutants and hazardous materials. It is used in this study to better
71 understand simulation results from Puff.

72 Besides parameter calibration, 1D plume models have been used to obtain global descriptors of volcanic
73 plumes. 1D plume models (e.g. Woods, 1988; Bursik, 2001; Mastin, 2007; de'Michieli Vitturi et al., 2015;
74 Folch et al., 2016; Pouget et al., 2016) solve the equations of motion in 1D using simplifying assumptions,
75 and hence depend on estimation of certain parameters, especially those related to the entrainment of air,
76 which is evaluated based on two coefficients: a coefficient due to turbulence in the rising buoyant jet, and
77 one due to the crosswind field. Different 1D models adopt different entrainment coefficients based on a
78 specific formulation or calibration against well-documented case studies. The feedback from plume to
79 atmosphere is usually ignored in 1D models. While these 1D models generated well-matched results with
80 3D models for plumes that are dominated by wind (often called weak plumes) much greater variability
81 is observed for strong plume scenarios (Bursik et al., 2009; Costa et al., 2016). On the other hand, 3D
82 numerical models for volcanic plumes based on first principles and having few parametrized coefficients
83 (Oberhuber et al., 1998; Neri et al., 2003; Suzuki et al., 2005; Cerminara et al., 2016a; Cao et al., 2018)
84 naturally create a 3D ash cloud, which could serve directly as an initial state of the volcanic material for
85 VATDs. However, there is no VATD simulation using such 3D ash clouds as initial conditions. In this paper,
86 we will carry out VATD simulations using an initial state for the ash cloud based on 3D plume simulations,
87 generated with Plume-SPH (Cao et al., 2018, 2017). The implementation techniques described in this paper
88 can be applied to any combination of VATD model and 3D plume model even though our investigation is
89 based on a specific VATD model and plume model.

90 The 1991 eruption of Pinatubo volcano is used as a case study. Pinatubo erupted between June 12 and 16,
91 1991, after weeks of precursory activity. The climactic phase started on June 15 at 0441 UTC and ended
92 around 1341 UTC (Holasek et al., 1996a). The climactic phase generated voluminous pyroclastic flows,
93 and sent Plinian and co-ignimbrite ash and gas columns to great altitudes (Scott et al., 1996). The evolution
94 of the Pinatubo ash and SO_2 clouds was tracked using visible (Holasek et al., 1996a), ultraviolet (Total
95 Ozone Mapping Spectrometer; TOMS) (Guo et al., 2004a) and infrared sensors, including the Advanced
96 Very High-Resolution Radiometer (AVHRR) (Guo et al., 2004b). There is sufficient observational data to
97 estimate the eruption conditions for the climactic phase of the eruption (Suzuki and Koyaguchi, 2009). The
98 availability of calibrated eruption conditions and extensive observational data regarding ash cloud transport
99 make the Pinatubo eruption an ideal case study.

2 MATERIALS AND METHODS

100 2.1 Plume-SPH Model

101 Plume-SPH (Cao et al., 2018) is designed to describe an injection of well mixed solid and volcanic gas
102 from a circular vent above a flat surface into a stratified stationary atmosphere. The basic assumptions of
103 the model are:

- 104 1. Molecular viscosity and heat conduction is neglected since turbulent energy and momentum exchange
105 are dominant.
- 106 2. Erupted material consisting of solid with different size and mixture of gases is assumed to be well
107 mixed and behave like a single phase fluid (phase 2) which is valid for eruptions with fine particles and
108 ash.

- 109 3. Air, which is assumed to be well mixed mixture of different gases, is assumed to be another phase
 110 (phase 1).
- 111 4. Assume thermodynamic equilibrium and dynamic equilibrium between the two phases. As a result,
 112 both phases share the common energy equation and momentum equations.
- 113 5. All other microphysical processes (such as the phase changes of H₂O aggregation, disaggregation,
 114 absorption of gas on the surface of solids, solution of gas into a liquid) and chemical processes are not
 115 considered in this model.
- 116 6. The effect of wind, is also not yet considered in this model.

Based on above assumptions, the governing equations of our model are given as:

$$\frac{\partial \rho}{\partial t} + \nabla \cdot (\rho \mathbf{v}) = 0 \quad (1)$$

$$\frac{\partial \rho \xi}{\partial t} + \nabla \cdot (\rho \xi \mathbf{v}) = 0 \quad (2)$$

$$\frac{\partial \rho \mathbf{v}}{\partial t} + \nabla \cdot (\rho \mathbf{v} \mathbf{v} + p \mathbf{I}) = \rho \mathbf{g} \quad (3)$$

$$\frac{\partial \rho E}{\partial t} + \nabla \cdot [(\rho E + p) \mathbf{v}] = \rho \mathbf{g} \cdot \mathbf{v} \quad (4)$$

117 where ρ is the density, \mathbf{v} is the velocity, ξ is the mass fraction of ejected material, \mathbf{g} is the gravitational
 118 acceleration, \mathbf{I} is a unit tensor. $E = e + K$ is the total energy which is a summation of kinetic energy K
 119 and internal energy e . An additional equation is required to close the system. In this model, the equation
 120 for closing the system is the following EOS (equation of state).

$$p = (\gamma_m - 1) \rho e \quad (5)$$

121 where

$$\gamma_m = R_m / C_{vm} + 1 \quad (6)$$

$$R_m = \xi_g R_g + \xi_a R_a \quad (7)$$

$$C_{vm} = \xi_s C_{vs} + \xi_g C_{vg} + \xi_a C_{va} \quad (8)$$

$$\xi_a = 1 - \xi \quad (9)$$

$$\xi_g = \xi \cdot \xi_{g0} \quad (10)$$

$$\xi_s = \xi - \xi_g \quad (11)$$

127 where, C_v is the specific heat with constant volume, R is the gas constant. ξ is the mass fraction of erupted
 128 material. The subscript m represents mixture of ejected material and air, s represents solid portion in the
 129 ejected material, g represents gas portion in the ejected material, a represents air, 0 represents physical
 130 properties of erupted material. ξ_{g0} is the mass fraction of vapor in the erupted material.

131 Three different boundary conditions are applied in this model. At the vent, temperature of erupted
 132 material T , eruption velocity \mathbf{v} , the mass fraction of vapor in erupted material ξ_{g0} and mass discharge
 133 rate \dot{M} are given. The pressure of erupted material p is assumed to be the same as ambient pressure for
 134 pressure-balanced eruption. The radius of vent is determined from ρ , \dot{M} and \mathbf{v} . Non-slip wall boundary
 135 condition is applied to the flat ground, where we enforce the velocity to be zero. With further assumption

136 that the ground is adiabatic, internal energy flux, which consists of heat flux and energy flux carried by
 137 mass flux, vanishes on the wall boundary. Pressure outlet boundary condition is applied to the surrounding
 138 atmosphere where the pressure is given. Except for the pressure, boundary values for density, velocity, and
 139 energy are determined by numerical calculation naturally. The initial condition for Plume-SPH is created
 140 based on atmosphere profile before the eruption.

141 The governing equations, EOS, boundary conditions, and initial conditions establish a complete mathe-
 142 matic model. The model is then discretized using smoothed particle hydrodynamics (SPH) method. The
 143 computational domain is discretized by SPH particles. The current version, Plume-SPH 1.0 (Cao et al.,
 144 2018), uses two types of SPH particles: 1) particles of phase 1 to represent ambient air, and 2) particles of
 145 phase 2 to represent erupted material. So before the eruption, the computational domain is fully occupied
 146 by particles of phase 1. During the eruption, particles of phase 2 are injected into the computational domain.
 147 The discretized model is then converted into computational software (Plume-SPH) based on a parallel data
 148 management framework (Cao et al., 2017).

149 The input parameters for Plume-SPH include the eruption condition at vent, the material properties, and
 150 atmosphere profile. The eruption parameters, material properties and atmosphere for the “Strong plume–no
 151 wind” case in the recent comparison study on eruptive column models (Costa et al., 2016) are adopted.
 152 Eruption conditions and material properties are listed in Table 3. Note that the density of erupted material
 153 at the vent and radius of the vent can be computed from the given parameters. The eruption pressure is
 154 assumed to be the same as the atmospheric pressure at the vent, hence is not given in the table. The vertical
 155 profiles of atmospheric properties were based on the reanalysis data from ECMWF (European Centre for
 156 Medium-Range Weather Forecasts) for the period corresponding to the climactic phase of the Pinatubo
 157 eruption.

158 Running of Plume-SPH essentially updates physics quantities, such as temperature, velocity, and the
 159 position of SPH particles in each time step. During Plume-SPH simulation, SPH particles of phase 2, which
 160 represent the erupted material, are injected from the eruption vent into the computation domain with an
 161 initial injection velocity. As they moving upwards, these particles will get mixed with SPH particles of
 162 phase 1, which represent the air, during the whole simulation. Their physics quantities get updated as well.
 163 After the simulation, the computation domain will be filled with SPH particles of both phase 1 and phase 2.
 164 Removing all SPH particles of phase 1 from the computation domain, all of the left SPH particles are these
 165 particles that represent the erupted material, which naturally forms a plume (see Fig. 1).

166 2.2 Puff and Initial Ash Cloud

167 Puff (Tanaka, 1991; Searcy et al., 1998) is a dynamic pollutant tracer model. the model is based on a 3D
 168 Lagrangian form of the fluid mechanics, in which the material transport is represented by the fluid motion,
 169 and diffusion is parameterized by a stochastic process of random walk. Here, the model is constructed by a
 170 sufficiently large number of Lagrangian tracer particles with a random variables $\mathbf{R}_i(t) = (x(t), y(t), z(t))$,
 171 where $i = 1 \sim M$, which represent position vectors of particles from the origin of the ash source at the
 172 time t . M is total number of Lagrangian tracer particles, a sample of all the ash particles.

$$173 \quad \mathbf{R}_i(t + \Delta t) = \mathbf{R}_i(t) + \mathbf{W}(t)\Delta t + \mathbf{Z}(t)\Delta t + \mathbf{S}_i(t)\Delta t \quad (12)$$

174 Here, \mathbf{W} accounts for wind advection, \mathbf{Z} is generated by Gaussian random numbers and accounts for
 175 turbulent dispersion, and \mathbf{S} is the terminal gravitational fallout velocity or settling speed, which depends on
 176 a tracer's size.

177 To start a Puff simulation, it requires a collection of tracer particles as the initial condition. The tracer
 178 particles has three basic properties, age, size and position. The age of each particle is the elapsed time
 179 from when they were released from the site. Ash particles in the initial ash cloud has zero ages. Ash size
 180 distribution is initialized using a Gaussian shape on a logarithmic scale. According to mean and standard
 181 deviation provided by user, Puff will assign size to each particle. Puff initialize the position of each particle
 182 according to semiempirical expressions. The height of each particle is determined according to specified
 183 distribution from the surface ($1000\text{mbar} \cong 0\text{m}$) to the top of the plume height, H_{max} , which is given by
 184 user. Puff also supports reading predefined initial ash cloud from a file, contains the coordinates of all
 185 tracer particles.

186 The commonly used distribution in Puff is Poisson distribution. For the Poisson distribution, the vertical
 187 height of ash particles is given by Eq. (13):

$$H = H_{max} - 0.5H_{width} * P + H_{width}R \quad (13)$$

188 where P is an integral value drawn from a Poisson distribution of unit mean, R is a uniformly distributed
 189 random number between 0 and 1, H_{max} is the maximum plume height, H_{width} represents an approximate
 190 vertical range over which the ash will be distributed. For Poisson distribution, two parameters, H_{max} and
 191 H_{width} controls the vertical ash distribution. Another commonly used vertical ash distribution in VATD
 192 simulation is Suzuki. For the Suzuki plume shape (Suzuki et al., 1983), the ash mass vertical distribution is
 193 assumed to follow the Eq. (Eq. (14)):

$$Q(z) = Q_m * \frac{k^2(1 - z/H_{max})\exp(k(z/H_{max} - 1))}{H_{max} [1 - (1 + k)\exp(-k)]} \quad (14)$$

194 Where Q_m is the total mass of erupted material, k is shape factor, which is an adjustable constant that
 195 controls ash distribution with height. A low value of k gives a roughly uniform distribution of mass with
 196 elevation, while high values of k concentrate mass near the plume top. For Suzuki distribution, besides
 197 the plume height H_{max} , there is another user specified parameter, k , which also affect the vertical ash
 198 distribution.

199 Puff initialize the horizontal distribution of ash particles according to semiempirical expression as well.
 200 Puff uses a uniformly distributed random process to determine ash particle locations in a circle centered
 201 on the volcano site. The maximum radius (at plume top) at which a particle can be located is given as
 202 “horizontal spread”. The horizontal displacement from a vertical line above the volcano is a random value
 203 within a circle of which the radius equals the “horizontal spread” multiplied by the ratio of the particle
 204 height H to the maximum H_{max} , see Eq. 15. So the resulting shape of the particle distribution within the
 205 plume is an inverted cone in which particles are located directly over the volcano at the lowest level and
 206 extend out further horizontally with increasing plume height.

$$r(H) = r_{max} * H/H_{max} * R \quad (15)$$

207 where $r(H)$ is the radius of the horizontal circle, whithin which, all particles at the height of H locate.
 208 r_{max} is the horizontal spread. H is the height, R is an uniformly distributed random number between 0 and
 209 1.

210 In summary, particle distributions in the initial ash cloud generated by semiempirical expressions are
 211 controlled by several parameters. Given user has chosen Poisson distribution for particle distribution in the

212 vertical direction, there are three user specified parameters that control the tracer particle distribution in
 213 the initial ash cloud: H_{max} , H_{width} , and r_{max} . User can optimize or calibrate these parameters to adjust
 214 the initial condition of Puff so that the simulated results match better with observations, such as satellite
 215 imagery or pilot reports. Besides the initial ash cloud, other input parameters for Puff are diffusivity in the
 216 vertical and horizontal directions, start and end time of the eruption, and eruption duration. When creating
 217 initial conditions from output of Plume-SPH, the total number of Lagrangian tracers is the count of all SPH
 218 particles of phase 2 in the plume. The same total number of Lagrangian tracers are used when creating
 219 initial ash cloud based on semiempirical expressions. All input parameters for Puff are list in Table 4.

220 2.3 Creation of Initial Ash Cloud From Plume-SPH Output

221 The steps to create an initial ash cloud based on the raw output of Plume-SPH are shown in Fig. 1.
 222 The method proposed consists in generating the initial ash cloud directly from Plume-SPH, foregoing
 223 assumptions and estimates, or inverse modeling, regarding ash injection height and timing. We use Plume-
 224 SPH as an example, noting that for other 3D plume models, the steps would be similar. The initial ash
 225 cloud is created from SPH particles of phase 2, which represents the erupted material in the model.

226 After reaching the maximum rise height and starting to spread horizontally, particles of phase 2 form an
 227 initial umbrella cloud (Fig. 2). The 3D plume simulation is considered complete once the umbrella cloud
 228 begins to form. Parcels that will be transported by the ambient wind are those above the “corner” region,
 229 where mean plume motion is horizontal rather than vertical.

230 Considering that SPH particles are only discretization points, each is assigned a grain size according to a
 231 given total grain size distribution (TGSD) (Paladio-Melosantos et al., 1996), and a concentration according
 232 to the mass and volumetric eruption rate. The Plume-SPH discretization points are thus switched to Puff
 233 Lagrangian tracer particles having grain sizes and concentrations. The coordinates of these tracer particles,
 234 which are initially in the local Cartesian coordinate system of Plume-SPH, are converted into Puff’s global
 235 coordinate system, which is given in terms of (*longitude*, *latitude*, *height*). Puff takes the initial ash
 236 cloud, consisting of the collection of Lagrangian tracer particles with grain size and concentration, and
 237 propagates from time t to time $t + \Delta t$ via solution to an advection/diffusion equation.

238 To summarize, there are four steps to create an initial ash cloud from the raw output of Plume-SPH:

- 239 1. filter by SPH particle type to select SPH particles that represent erupted material (phase 2)
- 240 2. filter by a mean velocity threshold to select the upper part (above the “corner” region) dominated by
 241 horizontal transport
- 242 3. switch SPH discretization points to Lagrangian tracer particles, by assigning grain size to each particle
- 243 4. convert coordinates of the SPH Lagrangian tracers into the VATDs’ geographic coordinate system

244 The features of the volcanic plume and resulting initial ash cloud used in the case study are shown in Fig. 2.
 245 It is important to point out that since both Plume-SPH and Puff are based on the Lagrangian method, there
 246 is no extra step of conversion between an Eulerian grid and Lagrangian particles.

247 2.4 Puff Restart

248 The plume and ash transport models are run at different time scales and length scales. The spatial and
 249 temporal resolutions of the plume simulations are much finer than those of the ash transport model. It takes
 250 tens of minutes (600s in this case) for the Pinatubo plume to reach a steady height. However the eruption
 251 persisted for a few hours (9 hours for the climactic phase of Pinatubo eruption), and it may be necessary
 252 to track ash transport for days following an eruption. At present, it is too expensive computationally to
 253 do 3D plume simulations of several hours in real time. In order to handle the difference in time scale, we

254 mimic a continuing eruption with intermittent pulses releasing ash particles. In particular, we restart Puff at
255 an interval of 600s, i.e., the physical time of the plume simulation to reach a steady height. At every Puff
256 restart, we integrate the output of the last Puff simulation and Plume-SPH into a new ash cloud. This new
257 ash cloud serves as a new initial condition with which to restart a Puff simulation. A sketch demonstrating
258 the overall restart process is shown in Fig. (3). The total number of Lagrangian tracer particles used in Puff
259 thus equals the summed number of particles in all releases. The total number of tracer particles is therefore
260 no longer a user-selected parameter. Fero et al. (2008) proposed using more realistic time-dependent plume
261 heights. We do not adopt that strategy here for simplicity, although the idea would be straightforward in
262 execution, given time-dependent eruption conditions.

3 RESULTS

263 Transport of volcanic ash resulting from the Pinatubo eruption on June 15, 1991, is simulated using two
264 different initial conditions. The first type of initial condition is created in a traditional way according to
265 key global descriptors (H_{max} , H_{width} and r_{max}) and the semiempirical plume shape expressions. We use
266 the observed top height (40km) and two other parameters assigned semiempirically (Bursik et al., 2012).
267 The second type of initial condition is created by the new method proposed in this paper. To create initial
268 conditions using the new method described in this paper, the plume rise is simulated first by Plume-SPH.
269 Then the initial ash cloud is obtained by processing the raw output of Plume-SPH following steps described
270 in Sec. 2.3. Except for initial conditions, the simulation parameters that control the VATD simulation are
271 the same for both simulations. Simulated ash transport results are compared against observations.

272 The simulation results using different initial conditions are compared with TOMS images and AVHRR
273 BTD ash cloud map imagery (Fig. 6). The differences between simulated ash transport by the “Semiempirical
274 initial cloud + Puff” and “Plume-SPH+ Puff” conditions are significant. The simulated ash concentration
275 based on the initial conditions created from Plume-SPH is qualitatively closer to observation than that
276 based on the semiempirical plume shape expression. At 23 hours and 31 hours after the beginning of the
277 climactic phase, the “Plume-SPH + Puff” simulation generates ash footprints that are closer to observations,
278 especially in forecasting the location where there is a high concentration of ash. However, ash just west of
279 Pinatubo observed in satellite images does not show up in “Plume-SPH + Puff” simulation results. This
280 disparity is likely due to the fact that Pinatubo continued erupting after the climactic phase, while we only
281 simulate the climactic phase. The “Semiempirical initial cloud + Puff” simulation, however, forecasts an
282 ash distribution more spatially restricted than observation. The location of the high concentration region
283 is far northwest of observation. Around 55 hours after the beginning of the climactic phase, the disparity
284 between observation and simulation becomes more obvious. Ash in the “Semiempirical initial cloud + Puff”
285 simulation is located too far west of the observation. The high concentration area of the “Plume-SPH +
286 Puff” simulation, even though closer to observation than that of the “Semiempirical initial cloud + Puff”
287 simulation, has also propagated further than observation.

288 Except for the initial conditions, both simulations adopt the same parameters and wind field data. That is
289 to say, the only difference between these two simulations is the initial distribution of ash parcels. The main
290 difference between simulation results from the “Plume-SPH + Puff” and the “Semiempirical initial cloud +
291 Puff” runs can be directly attributed to the initial ash particle distribution, which we discuss in detail in the
292 following section.

293 3.1 Importance of Maximum Height (H_{max})

294 In this section, we discuss the vertical distribution of ash particles in the initial ash cloud. The majority of
295 volcanic ash particles are usually injected at an elevation lower than the maximum height. For instance,

296 Holasek et al. (1996a,b) reported the maximum Pinatubo plume height as $\sim 39\text{ km}$ while the cloud heights
297 were estimated at $\sim 20 - 25\text{ km}$. Self et al. (1996) reported that the maximum plume height could have
298 been $> 35\text{ km}$, but that plume heights were $23 \sim 28\text{ km}$ after $\sim 15 - 16\text{ hours}$. The neutral buoyancy
299 height of the Pinatubo aerosol cloud was estimated with different methods at: $\sim 17 - 26\text{ km}$ (lidar) by
300 DeFoor et al. (1992), $\sim 20 - 23\text{ km}$ (balloon) by Deshler et al. (1992), $\sim 17 - 28\text{ km}$ (lidar) by Jäger
301 (1992), and $\sim 17 - 25\text{ km}$ (lidar) by Avdyushin et al. (1993). Based on comparison between simulated
302 clouds with early infrared satellite imagery of Pinatubo, Fero et al. (2008) reported that the majority of ash
303 was transported between 16 km and 18 km . These observations make good physical sense, as particles are
304 concentrated near the intrusion height of the umbrella cloud, not near the plume top, because the plume top
305 is due to momentum overshoot. However, the empirical expressions for the height-MER relation, which
306 are commonly adopted to create initial conditions for VATD simulations, tend to place the majority of ash
307 particles closer to the top if one uses observed maximum height in the empirical expressions.

308 Here we investigate two commonly used plume shapes, the Poisson and Suzuki. Particle distributions
309 (in terms of mass percentage or particle number percentage) in the vertical direction in the initial ash
310 cloud are shown in Fig. 7. In that figure, the vertical particle distribution based on Plume-SPH output is
311 compared with the vertical particle distribution created based on semiempirical shape expressions. Both
312 Poisson and Suzuki distributions in Fig. 7 take $H_{max} = 40\text{ km}$, which is close to the reported observation
313 of maximum height. When adopting the Poisson distribution, see (c) in Fig. 7, the majority of the particles
314 are between $30\text{ km} \sim 40\text{ km}$. Obviously, the Poisson function distributes the majority of ash at a higher
315 elevation than was observed (e.g. Fero et al., 2008). As for the Suzuki distribution, (d) in Fig. 7, the
316 majority of ash particles also occur in a range that is significantly higher than 25 km . As for initial ash
317 clouds based on Plume-SPH simulation, most ash particles are distributed between $\sim 17 - 28\text{ km}$, which
318 matches well with observations. The maximum height is also consistent with observation. To summarize,
319 using a semiempirical plume shape expression generates an unrealistic initial ash cloud even if we use the
320 observed maximum plume height.

321 For the Poisson and Suzuki distributions, the maximum in ash particles cannot be lower without changing
322 the maximum height. To distribute the majority of ash particles at a lower elevation, the maximum height
323 must be reduced to a value smaller than the observed maximum height. Adjusting parameters such as
324 maximum height in the empirical expression is actually the traditional source term calibration method. A
325 set of initial ash clouds using different maximum heights based on the Poisson distribution is shown in Fig.
326 8). The maximum heights adopted in plume shape expressions are not obtained from any plume model or
327 observation of plume height, but by *a posteriori* calibration to later-observed ash cloud transport heights.

328 The ash clouds created by the Poisson distribution with different maximum heights are used as initial
329 conditions in Puff simulations, whose results are shown in Fig. 11. Except for the maximum height, all
330 other parameters for creating an initial ash cloud are the same as those in Table 4. Of course, the range
331 over which the majority of ash particles is located is lower when using lower maximum heights. Figure
332 11 thus shows that the maximum height has a significant influence on the ash transport simulation. When
333 the maximum height is 10 km , the high concentration area lags behind that observed. If the designated
334 maximum height is 35 km , the high concentration area propagates faster and is more spatially confined than
335 observed. When using a maximum height of $\sim 41000\text{ m}$, the high concentration area propagates faster and
336 the footprint is narrower than in both observation and “Plume-SPH + Puff” simulation results (see Fig. 6).
337 The simulated high concentration area is closest to “Plume-SPH + Puff” simulation results when assigning
338 a maximum height of 30 km . The low-concentration front of the volcanic ash cloud propagates faster than
339 observed, and is located far west of the high concentration areas. A low concentration tail area also appears

in the simulation results while there is no such tail in the observed imagery, although this could be the result of imagery calibration or sensitivity. Simulation results based on a calibrated maximum height of 30 km show a footprint similar to those of “Plume-SPH + Puff”, although smaller in terms of area. However, the initial ash cloud created by a Poisson distribution with maximum height around 20 km generates the best match ash with observation. That is to say, a maximum height lower than the real maximum height is required by the Poisson plume shape to distribute ash particles at elevations comparable to the “true” ash distribution. Our hypothesis regarding the disparity between the “Semiempirical initial cloud + Puff” simulations and observation is confirmed. Since the initial condition of vertical ash distribution has such a dominant effect on VATD simulation, it is critical for the forecast capability of VATD simulations to explore more accurate and adaptive ways for establishing the initial ash distribution, especially methods that do not rely on *a posteriori* parameter calibration or inversion.

3.2 Effect of Vertical Spread (H_{width})

In the previous section, we explored the effects of adjusting the maximum height to change the vertical ash distribution at the source. In this section, we investigate the importance of another parameter in the semiempirical Poisson expression. We vary the “vertical spread” (H_{width} in Puff) in the range $\sim 3 - 10$ km. A set of initial ash clouds with different vertical spreads are shown in Fig. 8. Except for vertical spread, all other parameters for creating an initial ash cloud are the same as those in Table 4. The vertical width of the region within which the majority of ash particles are located becomes narrower when a smaller value for the vertical spread parameter is used, but changing it has no obvious effect on the height at which the largest fraction of ash particles is injected (essentially the height of a mode in ash distribution). The ash clouds based on different vertical spread parameters are then used as initial conditions in Puff simulations.

The results are shown in Fig. 11. Adjusting of the vertical spread changes particle distribution in the vertical direction, and thus, not surprisingly affects the VATD simulation results. None of the VATD simulations based on initial ash clouds with vertical spreads equal to 3, 5 or 10 km yield better results than do VATD simulations based on initial conditions created by Plume-SPH (see Fig. 11).

The calibration tests on vertical spread, carried out here, are certainly not exhaustive. One could do a more comprehensive calibration throughout the multi-dimensional parameter space (for Poisson distribution, the parameter space is two dimensional) and find better results. In addition, with a more complicated semiempirical plume shape expression, one could have more control over plume shape and might be able to get an initial condition that yields a more accurate ash transport forecast. However, more complicated and adaptable plume shape expressions imply a higher dimensional parameter space, which requires more effort in calibration, even though the degrees of freedom to adjust plume shape are still limited. Creating initial conditions based on 3D plume simulations is more adaptive to various cases and yields results as good as or better than calibration of the poorly-constrained semi-empirical parameter, vertical spread.

3.3 Horizontal Ash Distribution

The differences between the semiempirical plume particle distribution and actual (or simulated by the 3D plume model) are not only in the vertical direction. The importance of the horizontal distance of each initial ash particle from a line extending upward from the volcano is investigated in this section. Puff uses a uniformly distributed random process to determine ash particle locations in a circle centered on the volcano site as described in section 2.2. For the output of Plume-SPH, an effective (maximum) radius is determined according to a given threshold of ash concentration, following Cerminara et al. (2016b). A time averaged, spatial integration of the dynamic 3D flow field is conducted to remove significant fluctuations in time and space. Fig. 9 compares radius of the initial ash clouds created by 3D plume simulations with that assumed in the semiempirical plume shape expression adopted in Puff. It is impossible for the simple, assumed

384 plume shapes to capture the complex and more realistic shapes developed by Plume-SPH. Additional
385 parameterization may generate more reasonable shapes, but these would continue to be *ad hoc*, none would
386 likely to have the potential fidelity of the 3D simulation to reality, and adding a temporally changing
387 distribution would be difficult.

388 Comparison between cross-sectional views of the initial ash clouds is shown in Fig. 10. The cross-
389 sectional view of horizontal particle distribution using the semiempirical method (last figure in Fig. 10)
390 is similar to a cross-sectional view of a simulated 3D plume, in a general sense. However, for simulated
391 3D plumes, the ash particle distribution in cross section varies with height, which factor would become
392 increasingly important with increasing wind speed, were wind speed to be included in the estimate of initial
393 plume shape. It is difficult for the semiempirical expressions to accommodate such a complex distribution.

394 Despite the obvious difficulty of correctly estimating ash distribution near the vent, or for short propagation
395 times, assigning different values for the horizontal spread has a negligible effect on VATD simulation
396 results at large time. We investigated horizontal spread values between 50 km and 1600 km to create initial
397 ash clouds; all of them generated similar results at large propagation times (> 1 day). Figure 11 shows two
398 different simulation results based on initial ash clouds with horizontal spread equal to 50 km and 600 km,
399 respectively. No visible differences are apparent between them. This implies that horizontal distribution
400 has a less significant influence on VATD simulation results than does vertical distribution for long distance
401 or large time. Perhaps the most important ramification of this result is that it means the time at which the
402 “handshake” is made between Plume-SPH and the VATD does not affect results significantly for relatively
403 large distances and times.

4 DISCUSSION

4.1 Sensitivity Analysis of Other Parameters

405 Besides the positions of particles in the initial ash cloud, other parameters for Puff simulations are:
406 horizontal diffusivity, vertical diffusivity, mean grain size, grain size standard deviation and total number
407 of tracers. We present in this subsection informal but systematic sensitivity studies on these parameters.
408 We also investigate the influence of eruption duration. The sensitivity analyses will serve as the basis for
409 identifying possible sources of disparities between simulation and observation.

410 The sensitivity analyses illustrate that adjustment of parameters other than the positions of particles in
411 the initial ash cloud produces negligible visual differences in VATD simulation results. Using horizontal
412 diffusivities in the range of $[100, 100000] m^2 s^{-1}$ and vertical diffusivities in the range of $[1, 20] m^2 s^{-1}$
413 produces visually negligible differences. The simulated eruption duration should depend on either the total
414 observed duration or the duration of the climactic phase. We conducted several simulations with eruption
415 duration varying in the range of $[5, 11] hours$ with slightly different starting time of climactic phase. Table
416 2 lists all these simulations. However, only slight visible differences are observed among the simulated ash
417 transport outputs. The mean of the grain size distribution also has visually negligible effects on long-term
418 ash transport, according to our sensitivity tests in which we varied the log mean (base 10) grain radius in
419 the range of $[-7.3, -3.5] m$. The standard deviation, when varying in the range of $[0.1, 10] m$, generates a
420 negligible difference on long-range ash transport as well. A similar conclusion on parameter sensitivity is
421 reported by Fero et al. (e.g. 2008); Daniele et al. (e.g. 2009). Among the parameters explored, the eruption
422 duration and beginning time show the most obvious influence on simulated ash distribution, although the
423 effect is still small. To show the differences in an intuitive way, (a) - (c) in Fig. 4 shows simulated ash
424 distribution corresponding to 4.9 hours duration, 9 hours duration and 11 hours duration, respectively.
425 After 72 hours, relative to the simulation starting time, these three cases generate very similar results

426 with tiny visible differences. To summarize, all these parameters have negligible effects on long-term ash
427 distribution.

428 The new methodology for generating initial ash clouds introduces a new parameter: elevation threshold,
429 which is the lower elevation limit of the ash that will be transported by the VATD. This parameter needs to be
430 specified at this time, as there is no *a priori* way to define it, given the continuous vertical distribution of ash
431 in the eruption column. We carry out a separate, informal sensitivity analysis on this parameter by varying
432 the elevation threshold from 1500 m (the height of the vent) to 25000 m. The simulated ash distributions
433 show obvious visible differences. Such influence is especially obvious when the elevation threshold is
434 either very high or very low. However, varying the elevation threshold in the range of [12000, 18000] m
435 generates relatively small differences in ash transport simulation results. Figure 4 (d) and (e) compare the
436 simulated ash distributions corresponding to elevation thresholds of 1500 m and 15000 m. Compared with
437 the ash distribution for a threshold of 25000 m, an extra long tail appears when using an elevation threshold
438 of 1500 m. Adopting lower elevation thresholds adds more tracer particles at lower elevation. As the winds
439 at different elevations are different, the tracers at lower elevations propagate in different directions. The
440 HYSPLIT (Stein et al., 2015; Rolph et al., 2017) forward trajectory tracking starting at 1624 UTC on
441 June 15, indicates that the wind between elevations of 10000 m and 15000 m blew from north-east to
442 south-west, while winds of higher elevation blew from east to west (see Fig. 5). The results suggest that the
443 elevation threshold is best estimated from the height at which the parcel number or mass concentration has
444 an inflection point in the vertical distribution (*cf.* Figure 4(d) and (e)). Below this inflection point, particle
445 trajectories are primarily vertical in the stalk-like eruption column. Above this level, particle trajectories
446 are primarily horizontal, as they flow into the umbrella cloud gravity current.

447 The sensitivity analyses demonstrate that the initial conditions for the VATD simulations, derived from
448 the plume model, have the most significant effect on simulated ash propagation, while all other input
449 parameters have negligible influence. An initial ash cloud generated based on the semiempirical expressions,
450 e.g. Eq. 13 and Eq. 15, often differs significantly from a realistic initial ash cloud. Such initial conditions
451 might greatly compromise the accuracy of a VATD simulation.

452 In this paper, we do not carry out any sensitivity investigation with respect to wind field, even though it is
453 a dominant factor in a VATD simulation. In the present case study, we use global NOAA/OAR/ESRL6–
454 h , 2.0° reanalysis wind field data (Whitaker et al., 2004; Compo et al., 2006, 2011).

455 4.2 Summary

456 This paper presents, for the first time, VATD simulations using initial source conditions created by a 3D
457 plume model. Traditional VATD simulations use initial conditions created according to a semiempirical
458 plume shape expression. A case study of the 1991 Pinatubo eruption demonstrates that a 3D plume model
459 can create more realistic initial ash cloud and ash parcel positions, and therefore improve the accuracy of
460 ash transport forecasts. Informal sensitivity analyses suggest that initial conditions, as expressed in the
461 disposition of initial ash parcel positions in the vertical, have a more significant effect on a volcanic ash
462 transport forecast than most other parameters. Comparison of initial ash parcel distributions among the
463 3D plume model, semiempirical expressions, and observations suggests that a major subpopulation of ash
464 parcels should be placed at a much lower elevation than maximum height to obtain a better VATD forecast.
465 For the Pinatubo case study, “well-matched” simulation results are observed when using a maximum height
466 of around 30km in semiempirical expressions, which is much lower than the observed maximum height of
467 40km. Comparing the effects of the maximum height, vertical spread and horizontal spread shows that ash
468 particle distribution in the vertical direction has the strongest effect on VATD simulation.

469 To summarize, we have presented a novel method for creating *a priori* initial source conditions for
470 VATD simulations. We have shown that it might be possible to obtain initial positions of ash parcels
471 with deterministic forward modeling of the volcanic plume, potentially obviating or lessening the need to
472 attempt to somehow observe initial positions, or *a posteriori* create a history of release heights via inversion
473 (Stohl et al., 2011). Although the method now suffers from the high computational cost associated with
474 3D forward modeling, there is the possibility that in future it might not only help overcome shortcomings
475 of existing methods used to generate *a priori* input parameters, but also overcome the need to do the
476 thousands of runs associated with inverse modeling. In addition, computational cost will continue to
477 diminish as computing speed increases. As they are forward numerical models based on first principles,
478 3D plume models need little if any parameterization, and user intervention should not be required to
479 improve forecast power; no assumption about the initial position of ash parcels is needed. Generation of the
480 initial cloud of ash parcels directly by 3D simulation is potentially adaptable to a variety of volcanic and
481 atmospheric scenarios. In contrast, semiempirical expressions used to determine initial conditions require
482 several parameters to control ash particle distribution along a vertical line source or some simplified shape
483 of the initial ash cloud, making it difficult in some cases to generate initial conditions that closely resemble
484 a complex reality.

485 The full range of research issues raised by numerical forecasting of volcanic clouds is diverse. We
486 described in this paper the effect of initial conditions chosen from the output of a 3D plume model on
487 numerical forecasts of volcanic ash transport simulations. The wind field, another important factor in
488 volcanic ash transport simulations, is not discussed in the present work. Some other aspects, such as
489 microphysical processes, even though they play lesser roles, likely need to be included in VATDs to
490 improve accuracy for a particular eruption. In addition, eruption conditions are subject to change with time,
491 even during the climactic phase of an eruption. In the future, time-dependent initial conditions for VATDs
492 can be created from 3D plume simulations with time-dependent eruption conditions.

CONFLICT OF INTEREST STATEMENT

493 The authors declare that the research was conducted in the absence of any commercial or financial
494 relationships that could be construed as a potential conflict of interest.

AUTHOR CONTRIBUTIONS

495 The idea of using 3D plume model to start a VATD simulation originated from a conservation between AP
496 and MB. ZC carried out the Plume-SPH simulations, Puff simulations, results analysis, and prepared the
497 first draft. All authors worked together for further revisions. MB carried out the HYSPLIT simulation. QY
498 post processed the Puff simulation results, overlapped the simulation results with satellite observation. All
499 authors contributed equally to the manuscript writing. AP and MB obtained funding to financially support
500 the work.

FUNDING

501 This work was supported by National Science Foundation awards 1521855, 1621853, and 1821311,
502 1821338 and 2004302 and by the National Research Foundation Singapore and the Singapore Ministry
503 of Education under the Research Centres of Excellence initiative (project number: NRF2018NRF-
504 NSFC003ES-010).

ACKNOWLEDGMENTS

505 Support for the Twentieth Century Reanalysis Project dataset is provided by the U.S. Department of Energy,
506 Office of Science Innovative and Novel Computational Impact on Theory and Experiment (DOE INCITE)
507 program, and Office of Biological and Environmental Research (BER), and by the National Oceanic and
508 Atmospheric Administration Climate Program Office. We are grateful to the two anonymous reviewers of
509 the paper for their constructive comments and suggestions that improved the paper.

REFERENCES

- 510 Avdyushin, S., Tulinov, G., Ivanov, M., Kuzmenko, B., Mezhuev, I., Nardi, B., et al. (1993). 1. spatial and
511 temporal evolution of the optical thickness of the pinatubo aerosol cloud in the northern hemisphere
512 from a network of ship-borne and stationary lidars. *Geophysical research letters* 20, 1963–1966
- 513 Bonadonna, C., Connor, C. B., Houghton, B., Connor, L., Byrne, M., Laing, A., et al. (2005). Probabilistic
514 modeling of tephra dispersal: Hazard assessment of a multiphase rhyolitic eruption at tarawera, new
515 zealand. *Journal of Geophysical Research: Solid Earth* 110
- 516 Bonadonna, C. and Houghton, B. (2005). Total grain-size distribution and volume of tephra-fall deposits.
517 *Bulletin of Volcanology* 67, 441–456
- 518 Bursik, M. (2001). Effect of wind on the rise height of volcanic plumes. *Geophys. Res. Lett* 28, 3621–3624
- 519 Bursik, M., Jones, M., Carn, S., Dean, K., Patra, A., Pavolonis, M., et al. (2012). Estimation and
520 propagation of volcanic source parameter uncertainty in an ash transport and dispersal model: application
521 to the eyjafjallajokull plume of 14–16 april 2010. *Bulletin of volcanology* 74, 2321–2338
- 522 Bursik, M., Kobs, S., Burns, A., Braitseva, O., Bazanova, L., Melekestsev, I., et al. (2009). Volcanic
523 plumes and wind: Jetstream interaction examples and implications for air traffic. *Journal of Volcanology*
524 and *Geothermal Research* 186, 60–67
- 525 Cao, Z., Patra, A., Bursik, M., Pitman, E. B., and Jones, M. (2018). Plume-sph 1.0: a three-dimensional,
526 dusty-gas volcanic plume model based on smoothed particle hydrodynamics. *Geoscientific Model
527 Development* 11, 2691–2715
- 528 Cao, Z., Patra, A., and Jones, M. (2017). Data management and volcano plume simulation with parallel
529 sph method and dynamic halo domains. *Procedia Computer Science* 108, 786–795
- 530 Cerminara, M., Esposti Ongaro, T., and Berselli, L. (2016a). Ashee-1.0: a compressible, equilibrium-
531 eulerian model for volcanic ash plumes. *Geoscientific Model Development* 9, 697–730
- 532 Cerminara, M., Esposti Ongaro, T., and Neri, A. (2016b). Large eddy simulation of gas–particle kinematic
533 decoupling and turbulent entrainment in volcanic plumes. *Journal of Volcanology and Geothermal
534 Research*
- 535 Compo, G. P., Whitaker, J. S., and Sardeshmukh, P. D. (2006). Feasibility of a 100-year reanalysis using
536 only surface pressure data. *Bulletin of the American Meteorological Society* 87, 175–190
- 537 Compo, G. P., Whitaker, J. S., Sardeshmukh, P. D., Matsui, N., Allan, R. J., Yin, X., et al. (2011). The
538 twentieth century reanalysis project. *Quarterly Journal of the Royal Meteorological Society* 137, 1–28
- 539 Costa, A., Suzuki, Y., Cerminara, M., Devenish, B., Esposti Ongaro, T., Herzog, M., et al. (2016). Results
540 of the eruptive column model inter-comparison study. *Journal of Volcanology and Geothermal Research*
- 541 D'amours, R. (1998). Modeling the etex plume dispersion with the canadian emergency response model.
542 *Atmospheric Environment* 32, 4335–4341
- 543 Daniele, P., Lirer, L., Petrosino, P., Spinelli, N., and Peterson, R. (2009). Applications of the puff model to
544 forecasts of volcanic clouds dispersal from etna and vesuvio. *Computers & Geosciences* 35, 1035–1049
- 545 DeFoor, T. E., Robinson, E., and Ryan, S. (1992). Early lidar observations of the june 1991 pinatubo
546 eruption plume at mauna loa observatory, hawaii. *Geophysical research letters* 19, 187–190

- 547 de'Michieli Vitturi, M., Neri, A., and Barsotti, S. (2015). Plume-mom 1.0: A new integral model of
548 volcanic plumes based on the method of moments. *Geoscientific Model Development* 8, 2447–2463
- 549 Deshler, T., Hofmann, D., Johnson, B., and Rozier, W. (1992). Balloonborne measurements of the pinatubo
550 aerosol size distribution and volatility at laramie, wyoming during the summer of 1991. *Geophysical*
551 *research letters* 19, 199–202
- 552 Draxler, R. R. and Hess, G. (1998). An overview of the hysplit_4 modelling system for trajectories.
553 *Australian meteorological magazine* 47, 295–308
- 554 Fero, J., Carey, S. N., and Merrill, J. T. (2008). Simulation of the 1980 eruption of mount st. helens using
555 the ash-tracking model puff. *Journal of Volcanology and Geothermal Research* 175, 355–366
- 556 Fero, J., Carey, S. N., and Merrill, J. T. (2009). Simulating the dispersal of tephra from the 1991
557 pinatubo eruption: implications for the formation of widespread ash layers. *Journal of Volcanology and*
558 *Geothermal Research* 186, 120–131
- 559 Folch, A., Costa, A., and Macedonio, G. (2009). Fall3d: A computational model for transport and
560 deposition of volcanic ash. *Computers & Geosciences* 35, 1334–1342
- 561 Folch, A., Costa, A., and Macedonio, G. (2016). Fplume-1.0: An integral volcanic plume model accounting
562 for ash aggregation. *Geoscientific Model Development* 9, 431
- 563 Guo, S., Bluth, G. J., Rose, W. I., Watson, I. M., and Prata, A. (2004a). Re-evaluation of so2 release
564 of the 15 june 1991 pinatubo eruption using ultraviolet and infrared satellite sensors. *Geochemistry,*
565 *Geophysics, Geosystems* 5
- 566 Guo, S., Rose, W. I., Bluth, G. J., and Watson, I. M. (2004b). Particles in the great pinatubo volcanic cloud
567 of june 1991: The role of ice. *Geochemistry, Geophysics, Geosystems* 5
- 568 Heffter, J. L. and Stunder, B. J. (1993). Volcanic ash forecast transport and dispersion (vaftad) model.
569 *Weather and forecasting* 8, 533–541
- 570 Holasek, R., Self, S., and Woods, A. (1996a). Satellite observations and interpretation of the 1991 mount
571 pinatubo eruption plumes. *Journal of Geophysical Research: Solid Earth* 101, 27635–27655
- 572 Holasek, R. E., Woods, A. W., and Self, S. (1996b). Experiments on gas-ash separation processes in
573 volcanic umbrella plumes. *Journal of volcanology and geothermal research* 70, 169–181
- 574 Jäger, H. (1992). The pinatubo eruption cloud observed by lidar at garmisch-partenkirchen. *Geophysical*
575 *research letters* 19, 191–194
- 576 Mastin, L. G. (2007). A user-friendly one-dimensional model for wet volcanic plumes. *Geochemistry,*
577 *Geophysics, Geosystems* 8
- 578 Neri, A., Esposti Ongaro, T., Macedonio, G., and Gidaspow, D. (2003). Multiparticle simulation of
579 collapsing volcanic columns and pyroclastic flow. *Journal of Geophysical Research: Solid Earth*
580 (1978–2012) 108
- 581 Oberhuber, J. M., Herzog, M., Graf, H.-F., and Schwanke, K. (1998). Volcanic plume simulation on large
582 scales. *Journal of Volcanology and Geothermal Research* 87, 29–53
- 583 Paladio-Melosantos, M. L. O., Solidum, R. U., Scott, W. E., Quiambao, R. B., Umbal, J. V., Rodolfo, K. S.,
584 et al. (1996). Tephra falls of the 1991 eruptions of mount pinatubo. *Fire and mud* 12000, 12030
- 585 Pouget, S., Bursik, M., Singla, P., and Singh, T. (2016). Sensitivity analysis of a one-dimensional model of
586 a volcanic plume with particle fallout and collapse behavior. *Journal of Volcanology and Geothermal*
587 *Research*
- 588 Rolph, G., Stein, A., and Stunder, B. (2017). Real-time environmental applications and display system:
589 Ready. *Environmental Modelling & Software* 95, 210–228
- 590 Schwaiger, H. F., Denlinger, R. P., and Mastin, L. G. (2012). Ash3d: A finite-volume, conservative
591 numerical model for ash transport and tephra deposition. *Journal of Geophysical Research: Solid Earth*

- 592 117
- 593 Scott, W. E., Hoblitt, R. P., Torres, R. C., Self, S., Martinez, M. M. L., and Nillos, T. (1996). Pyroclastic
594 flows of the june 15, 1991, climactic eruption of mount pinatubo. *Fire and Mud: eruptions and lahars of*
595 *Mount Pinatubo, Philippines* , 545–570
- 596 Searcy, C., Dean, K., and Stringer, W. (1998). Puff: A volcanic ash tracking and prediction model. *Journal*
597 *of Volcanology and Geothermal Research* 80, 1–16
- 598 Self, S., Zhao, J.-X., Holasek, R. E., Torres, R. C., and King, A. J. (1996). The atmospheric impact of the
599 1991 mount pinatubo eruption
- 600 Stein, A., Draxler, R., Rolph, G., Stunder, B., Cohen, M., and Ngan, F. (2015). Noaa's hysplit atmospheric
601 transport and dispersion modeling system. *Bulletin of the American Meteorological Society* 96, 2059–
602 2077
- 603 Stohl, A., Prata, A., Eckhardt, S., Clarisse, L., Durant, A., Henne, S., et al. (2011). Determination of
604 time-and height-resolved volcanic ash emissions and their use for quantitative ash dispersion modeling:
605 the 2010 eyjafjallajökull eruption. *Atmospheric Chemistry and Physics* 11, 4333–4351
- 606 Suzuki, T. et al. (1983). A theoretical model for dispersion of tephra. *Arc volcanism: physics and tectonics*
607 95, 113
- 608 Suzuki, Y. and Koyaguchi, T. (2009). A three-dimensional numerical simulation of spreading umbrella
609 clouds. *Journal of Geophysical Research: Solid Earth (1978–2012)* 114
- 610 Suzuki, Y. J., Koyaguchi, T., Ogawa, M., and Hachisu, I. (2005). A numerical study of turbulent mixing
611 in eruption clouds using a three-dimensional fluid dynamics model. *Journal of Geophysical Research:*
612 *Solid Earth* 110
- 613 Tanaka, H. (1991). Development of a prediction scheme for the volcanic ash fall from redoubt volcano. In
614 *First Int'l. Symp. on Volcanic Ash and Aviation Safety*. vol. 58
- 615 Tupper, A., Itikarai, I., Richards, M., Prata, F., Carn, S., and Rosenfeld, D. (2007). Facing the challenges of
616 the international airways volcano watch: the 2004/05 eruptions of manam, papua new guinea. *Weather*
617 *and Forecasting* 22, 175–191
- 618 Walko, R., Tremback, C., and Bell, M. (1995). Hypact: The hybrid particle and concentration transport
619 model. *User's guide*
- 620 Whitaker, J. S., Compo, G. P., Wei, X., and Hamill, T. M. (2004). Reanalysis without radiosondes using
621 ensemble data assimilation. *Monthly Weather Review* 132, 1190–1200
- 622 Witham, C., Hort, M., Potts, R., Servranckx, R., Husson, P., and Bonnardot, F. (2007). Comparison of
623 vaac atmospheric dispersion models using the 1 november 2004 grimsvötn eruption. *Meteorological*
624 *Applications* 14, 27–38
- 625 Woods, A. (1988). The fluid dynamics and thermodynamics of eruption columns. *Bulletin of Volcanology*
626 50, 169–193
- 627 Zidikheri, M. J., Lucas, C., and Potts, R. J. (2017). Estimation of optimal dispersion model source
628 parameters using satellite detections of volcanic ash. *Journal of Geophysical Research: Atmospheres*
629 122, 8207–8232

FIGURE CAPTIONS

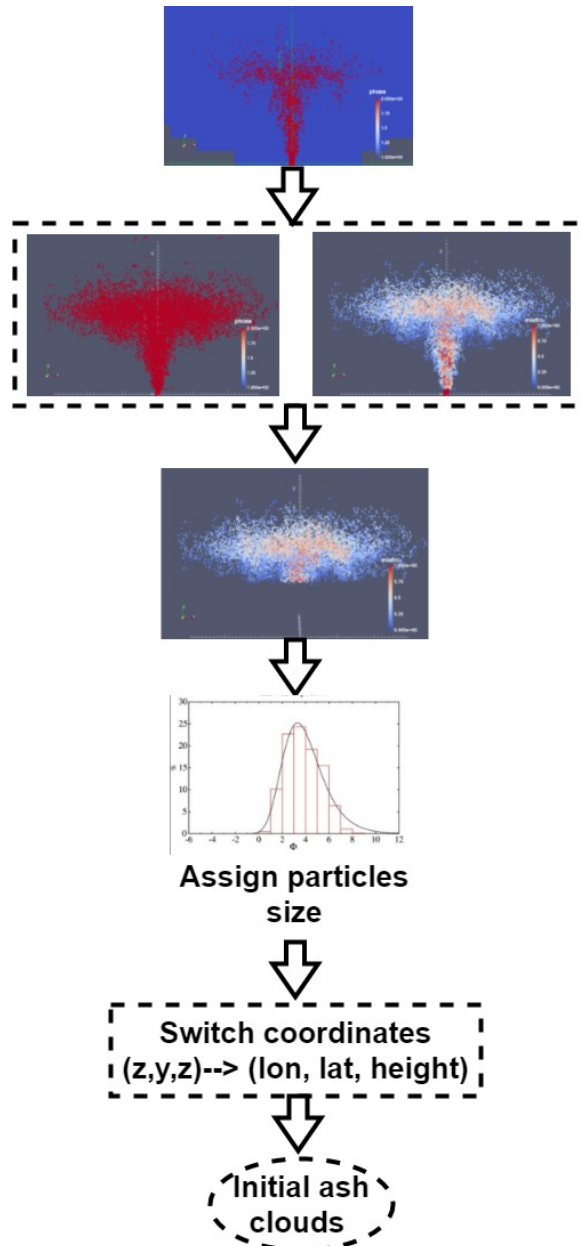


Figure 1. Steps to create initial condition for Puff based on raw output of Plume-SPH (Cao et al., 2018). First row: raw output of Plume-SPH. Blue particles are phase 1 (ambient air), red particles are phase 2 (erupted material). Second row: plume after removing SPH particles of phase 1. Picture at right is colored according to the mass fraction of erupted material. Third row: volcanic plume above the “corner” region after cutting off the lower portion. Fourth row: assign sizes to particles converting numerical discretization points into tracers. Fifth row: switch coordinates in local coordinate system into (*longitude, latitude, height*)

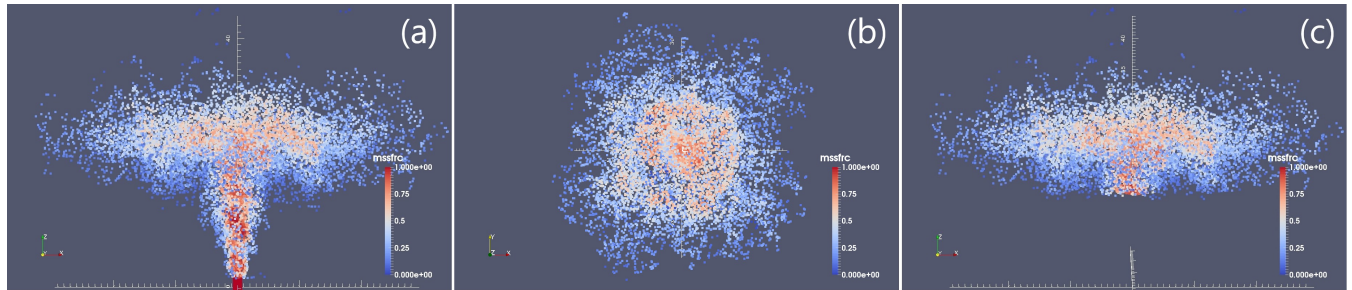


Figure 2. Volcano plume from 3D plume model. All particles in the pictures are of phase 2 (particle of phase 1 has been removed) at 600s after eruption, at which time, the plume has already reached the maximum height and started spreading radially. (a) is front view of the whole plume. (b) top view of the plume. (c) is front view of the initial ash cloud, which is essentially a portion of the whole plume with elevation higher than a given threshold (in this picture is 15000m). Particles are colored according to mass fraction of erupted material. Red represents high mass fraction while blue represents low mass fraction.

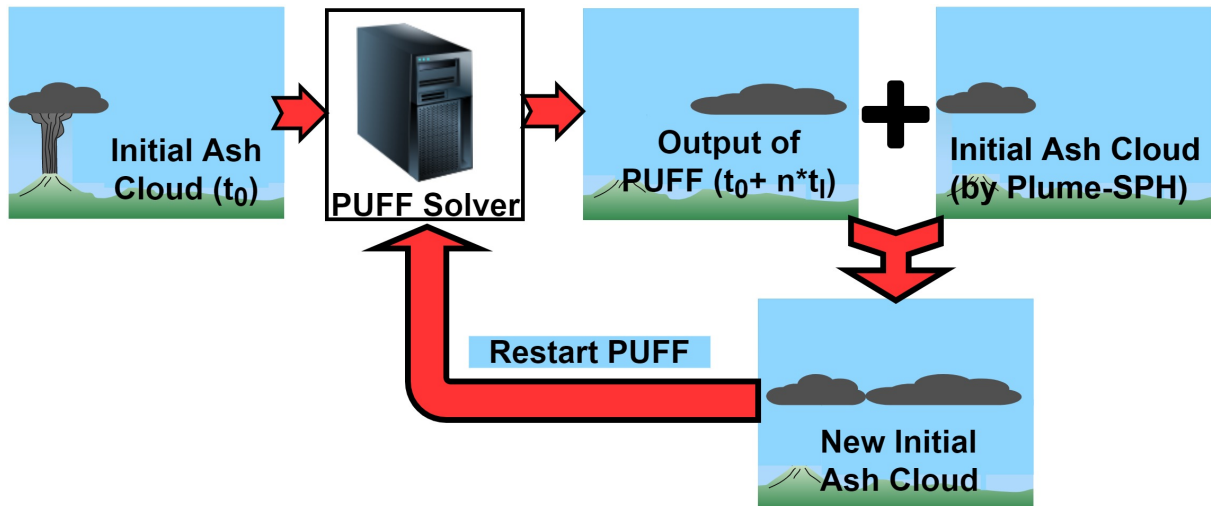


Figure 3. Mimic successive eruption with intermittent pulsed releasing of ash particles. t_I is the period of pulsing release. t_I equals the physical time of 3D plume simulation.

Table 1. Three different methods for creating initial conditions (initial ash clouds) for Puff simulation

	No model	1D model	3D model
Maximum height	Calibration	Semiempirical	1st principle
Average height	Calibration	Conservation laws (1D)	1st principle
Vertical spread	Calibration	Semiempirical	1st principle
Column radius	Calibration	Conservation laws (1D)	1st principle
Plume shape	Semiempirical	Semiempirical	1st principle
Tracers number	Free parameter	Free Parameter	Based on simulation

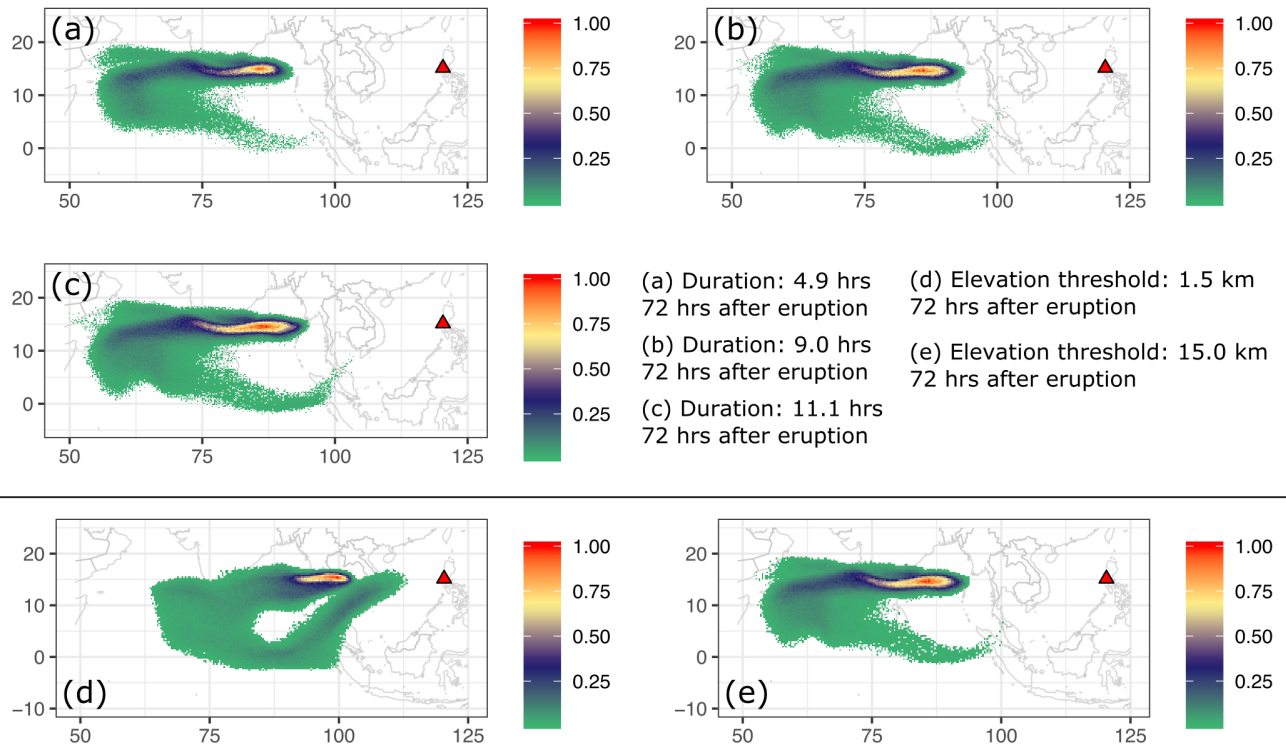


Figure 4. Sensitivity of Puff simulation with respect to eruption durations and initial ash cloud cutoff heights .(a) to (c) are simulated ash distribution with different starting and ending time. They corresponding to eruption duration of 4.9 hours, 9 hours and 11.1 hours respectively. Starting and ending time for each case is in Table 2. (d) and (e) are simulated ash distribution taking initial ash clouds obtained using different elevation thresholds (1500m and 15000 m) from output of Plume-SPH. The starting and ending time are corresponding to 9 hours duration case in Table 2. The contours correspond to ash concentration at 72 hours after eruption.

Table 2. The starting and ending time (UT) for simulating the climactic phase of Pinatubo eruption on June 15 1991. Observed plume height (Holasek et al., 1996a) at different time are also listed in the table.

Eruption duration	4.9 hours	9 hours	10 hours	11.1 hours
Start time	0441	0441	0441	0334
Height at start time	37.5 km	37.5 km	37.5 km	24.5 km
End time	0934	1341	1441	1441
Height at end time	35 km	26.5 km	22.5	22.5 km

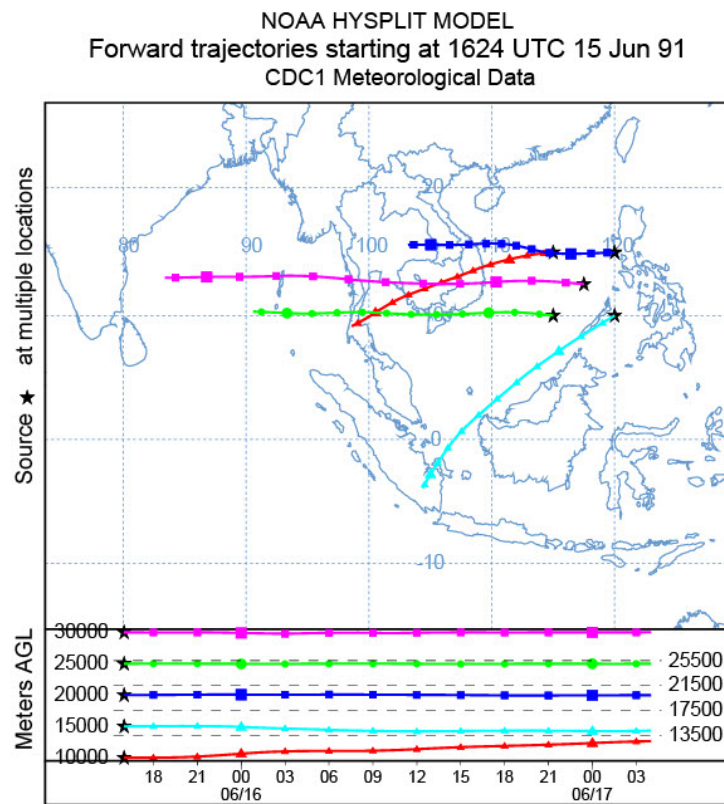


Figure 5. Trajectories of particles starting from different heights indicating the wind directions of different evaluations.

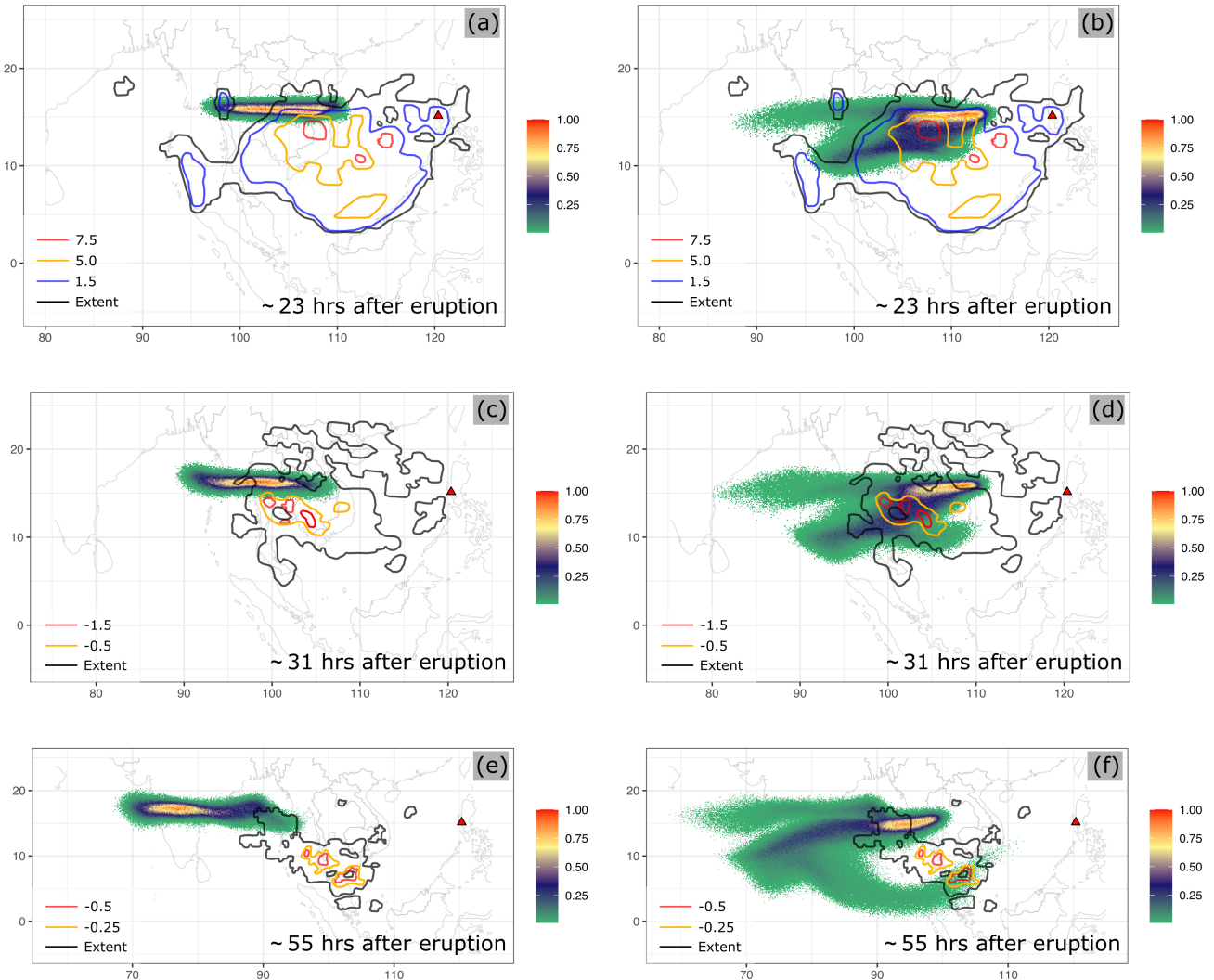


Figure 6. Comparison between “Semiempirical initial cloud + Puff” and “Plume-SPH + Puff”. Pictures to the left are: Puff simulation based on initial condition created according to semiempirical plume shape expression. Pictures to the right are Puff simulation based on initial condition generated by Plume-SPH. TOMS or AVHRR image of Pinatubo ash cloud are overlapped with the simulation results. Ash clouds at different hours after eruption are on different rows. From top to bottom, the images are corresponding to around 23 hours after eruption (UT 199106160341), 31 hours after eruption (UT 199106161141), 55 hours after eruption (UT 199106171141). The observation data on the first row are TOMS ash and ice map. The observation data on the second and third row are AVHRR BTD ash cloud map with atmospheric correction method applied (Guo et al., 2004b).

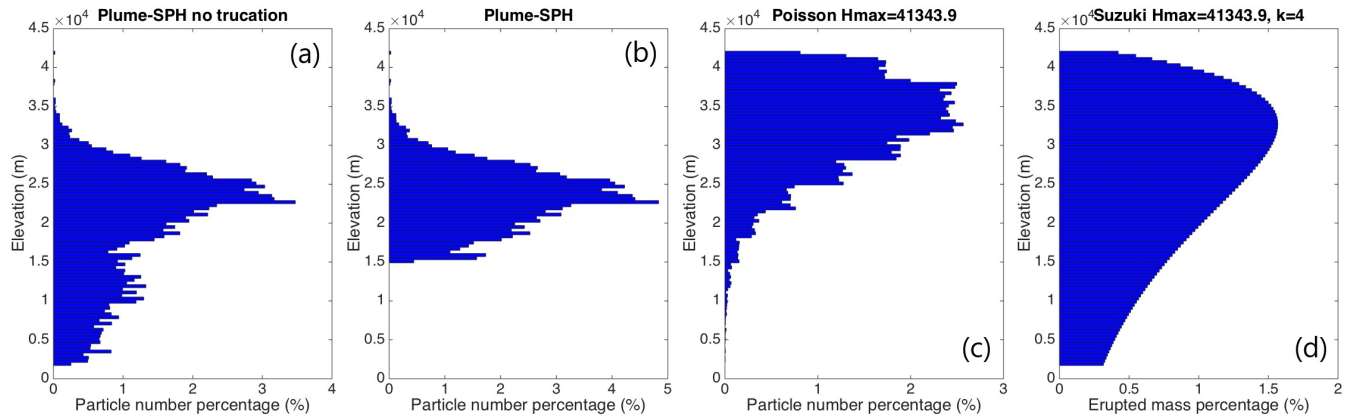


Figure 7. Particle distribution of initial ash cloud in vertical direction. (a) is corresponding to the initial ash cloud obtained from Plume-SPH output. (b) is corresponding to ash distribution of Plume-SPH output truncated by a elevation threshold of 15000m. (c) is for vertical ash distribution based on Poisson distribution with maximum height equals to 40000m. Another parameter, the vertical spread, in the expression of Poisson plume shape is 6662m. (d) is corresponding to Suzuki distribution with maximum height equals to 40000m. Another parameter in Suzuki distribution, the shape factor, is 4. The x axis is the percentage of particle numbers for Plume-SPH and Poisson. For Suzuki the x axis is the mass percentage of erupted material.

Table 3. List of eruption condition and material properties for plume simulation

Parameters	Units	Plume
Vent velocity	$m \cdot s^{-1}$	275
Vent gas mass fraction		0.05
Vent Temperature	K	1053
Vent height	m	1500
Mass discharge rate	$kg \cdot s^{-1}$	1.5×10^9
Specific heat of gas at constant volume	$J \cdot kg^{-1} \cdot K^{-1}$	717
Specific heat of air at constant volume	$J \cdot kg^{-1} \cdot K^{-1}$	1340
Specific heat of solid	$J \cdot kg^{-1} \cdot K^{-1}$	1100
Specific heat of gas at constant pressure	$J \cdot kg^{-1} \cdot K^{-1}$	1000
Specific heat of air at constant pressure	$J \cdot kg^{-1} \cdot K^{-1}$	1810
Density of air at vent height	$kg \cdot m^{-3}$	1.104
Pressure at vent height	Pa	84363.4

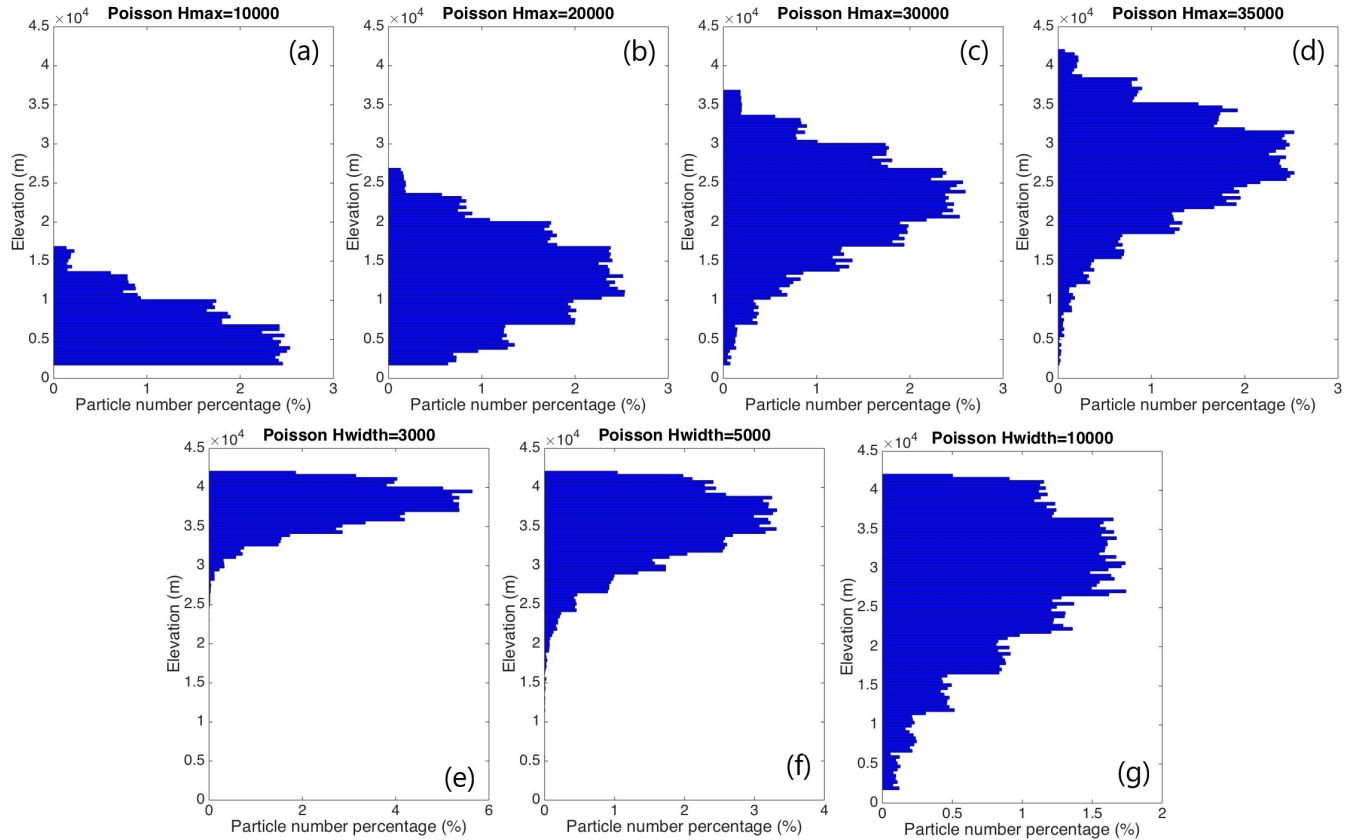


Figure 8. Initial particle distribution in vertical direction based on Poisson plume shape. The first row varies maximum heights. (a) to (d) are corresponding to maximum height of 10000m, 20000m, 30000m, 35000m. Another parameter, the vertical spread, in the expression of Poisson plume shape is 6662m for all four figures in the first row. The second row varies “vertical spread”. (e) to (g) are corresponding to vertical spread of 3km, 5km and 10km. The maximum height in the expression of Poisson plume shape is 40000m for all three figures. The x axis is the percentage of particle numbers. See Fig. 7 for vertical ash distribution of Plume-SPH output.

Table 4. Parameters used in VATD simulation of the climactic phase of Pinatubo eruption on June 15 1991. The first six parameters are used by semiempirical expression to create an initial ash cloud. When creating an initial condition based on the Plume-SPH model, these parameters are extracted from output of Plume-SPH model.

Parameters	Unit	Semiempirical	Plume-SPH
Maximum Height (H_{max})	m	40000	-
Horizontal Spread (r_{max})	km	103.808	-
Vertical Spread (H_{width})	km	6.662	-
Plume Shape	-	Poisson	-
Total Ash Particles	-	1768500	1768500
Elevation Threshold	m	-	15000
Horizontal Diffusivity	m^2/s	10000	10000
Vertical Diffusivity	m^2/s	10	10
Grain Size Distribution	-	Gaussian	Gaussian
Mean of Grain Size (Radius)	mm	3.5×10^{-2}	3.5×10^{-2}
Standard Deviation of Grain Size	-	1.0	1.0
Start Time	UT	0441	0441
End time	UT	1341	1341
Simulation Duration	hour	72	72

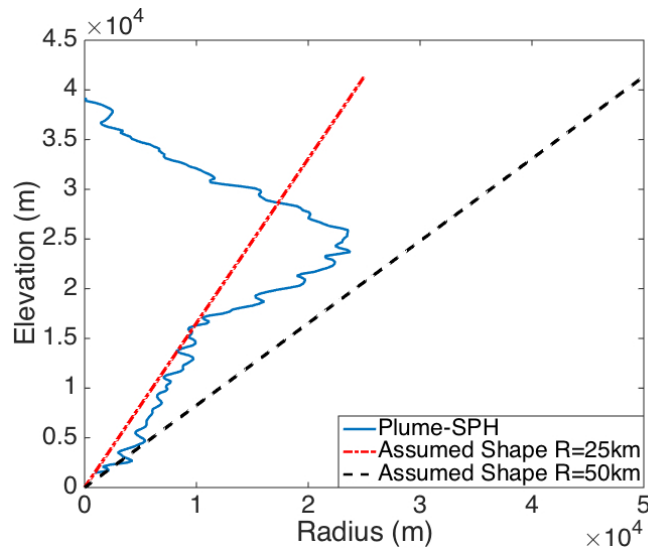


Figure 9. Comparison between radius of initial ash clouds created by 3D plume model (Plume-SPH) and assumed initial ash cloud shape in Puff. The plume shape expression used in Puff defines an inverted cone whose actual shape changes when “horizontal spread” takes different values. $R = 25\text{km}$ is corresponding to “horizontal spread” equals to 50km . $R = 50\text{km}$ is corresponding to “horizontal spread” equals to 100km

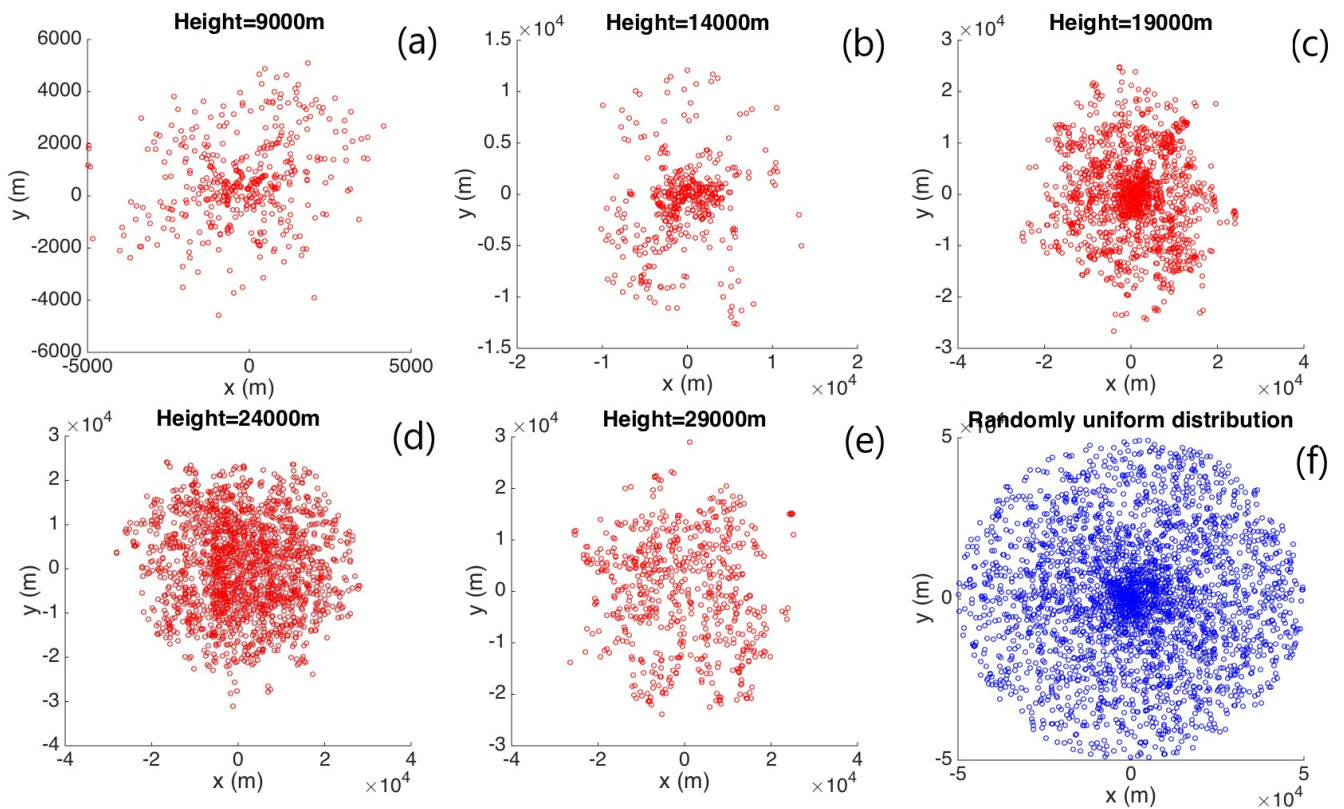


Figure 10. Horizontal distribution of ash particles (tracers) on a cross section of initial ash cloud. Puff assumes a randomly uniform distribution of ash particles within a circle, as shown by blue dots in (f). All other figures show the ash particle distribution of initial ash clouds created by Plume-SPH at different elevations.

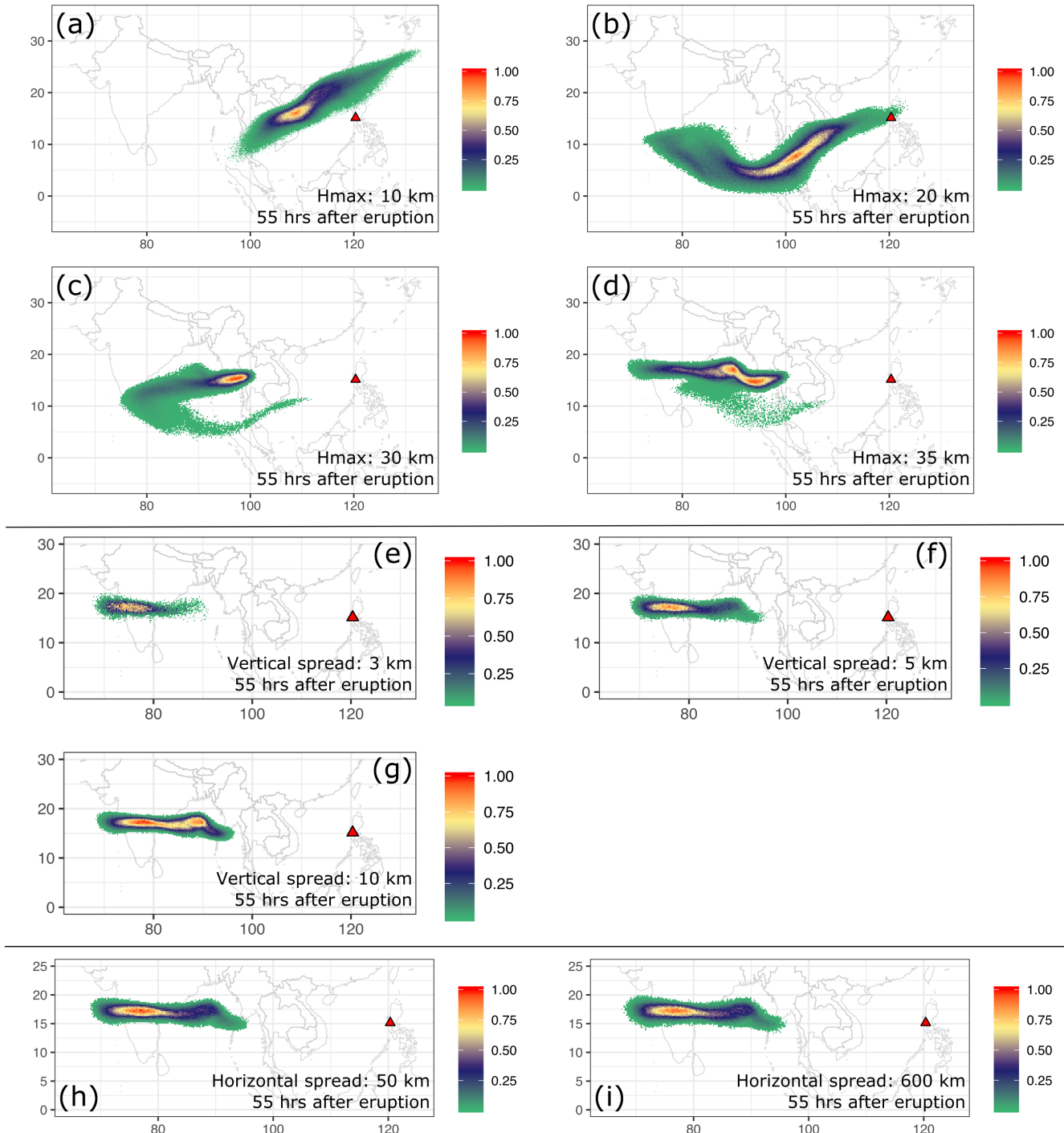


Figure 11. Ash transport simulated by Puff using different initial ash clouds created according the empirical expressions. Initial ash cloud for (a) to (d) are created according to Poisson distribution with maximum plume heights of 10km, 20km, 30km and 35km respectively. Initial ash cloud for (e) to (g) are created with vertical spread equals to 3km, 5km and 10km. respectively. Initial ash cloud for (h) - (i) are created with “horizontal spread” equals to 50km and 600km respectively. All images are for simulated ash transport around 55 hours after eruption (UT 199106171141). See the observed cloud image in Fig. 6.